

This discussion paper is/has been under review for the journal Atmospheric Chemistry and Physics (ACP). Please refer to the corresponding final paper in ACP if available.

Chemical aging of *m*-xylene secondary organic aerosol: laboratory chamber study

C. L. Loza¹, P. S. Chhabra^{1,*}, L. D. Yee², J. S. Craven¹, R. C. Flagan^{1,2}, and J. H. Seinfeld^{1,2}

¹Division of Chemistry and Chemical Engineering, California Institute of Technology, Pasadena, CA, USA

²Division of Engineering and Applied Science, California Institute of Technology, Pasadena, CA, USA

*now at: Aerodyne Research, Inc., Billerica, MA, USA

Received: 20 August 2011 – Accepted: 3 September 2011 – Published: 7 September 2011

Correspondence to: J. H. Seinfeld (seinfeld@caltech.edu)

Published by Copernicus Publications on behalf of the European Geosciences Union.

Title Page

Abstract

Introduction

Conclusions

References

Tables

Figures

◀

▶

◀

▶

Back

Close

Full Screen / Esc

Printer-friendly Version

Interactive Discussion



Abstract

Secondary organic aerosol (SOA) can reside in the atmosphere for a week or more. While its initial formation from the gas-phase oxidation of volatile organic compounds tends to take place in the first few hours after emission, SOA can continue to evolve chemically over its atmospheric lifetime. Simulating this chemical aging over an extended time in the laboratory has proven to be challenging. We present here a procedure for studying SOA aging in laboratory chambers that is applied to achieve 36 h of oxidation. The formation and evolution of SOA from the photooxidation of *m*-xylene under low-NO_x conditions and in the presence of either neutral or acidic seed particles is studied. In SOA aging, increasing molecular functionalization leads to less volatile products and an increase in SOA mass, whereas gas-phase or particle-phase fragmentation chemistry results in more volatile products and a loss of SOA. The challenge is to discern from measured chamber variables the extent to which these processes are important for a given SOA system. In the experiments conducted, *m*-xylene SOA mass increased over the initial 12-h of photooxidation and decreased beyond that time. The oxidation of the SOA, as manifested in the O:C elemental ratio and fraction of organic ion detected at *m/z* 44 measured by the Aerodyne aerosol mass spectrometer, decreased during the first 5 h of reaction, reached a minimum, and then increased continuously until the 36 h termination. This behavior is consistent with an initial period in which, as the mass of SOA increases, products of higher volatility partition to the aerosol phase, followed by an aging period in which gas- and particle-phase reaction products become increasingly more oxidized. After about 12–13 h, the SOA mass reaches a maximum and decreases, suggesting the existence of fragmentation chemistry. When irradiation is stopped 12.4 h into one experiment, and OH generation ceases, no loss of SOA is observed, indicating that the loss of SOA is either light- or OH-induced. Chemical ionization mass spectrometry measurements of low-volatility *m*-xylene oxidation products exhibit behavior indicative of continuous photooxidation chemistry. A condensed chemical mechanism of *m*-xylene oxidation under low-NO_x

m-Xylene SOA aging

C. L. Loza et al.

Title Page

Abstract

Introduction

Conclusions

References

Tables

Figures



Back

Close

Full Screen / Esc

Printer-friendly Version

Interactive Discussion



conditions is capable of reproducing the general behavior of gas-phase evolution observed here. Moreover, order of magnitude analysis of the mechanism suggests that gas-phase OH reaction of low volatility SOA precursors is the dominant pathway of aging in the *m*-xylene system although OH reaction with particle surfaces cannot be ruled out.

1 Introduction

Organic aerosol (OA) constitutes 20–90 % of all submicron particles in the atmosphere, and up to 80 % of this is classified as secondary organic aerosol (SOA) (Zhang et al., 2007; Murphy et al., 2006). Aerosol particles in the atmosphere can have lifetimes of 5–12 days (Balkanski et al., 1993), during which they can undergo continuous physical and chemical processing, commonly called aging (Rudich et al., 2007). Laboratory experiments designed to study SOA formation typically have a duration of up to 1 day, during which all processes that cause ambient particle aging may not be captured. Chemical aging of SOA can affect gas-particle partitioning through processes such as vapor-phase oxidation of semivolatiles, heterogeneous oxidation, and reactions within the particle phase, e.g. oligomerization, that take place on a fairly long timescale (Kroll and Seinfeld, 2008; Hallquist et al., 2009).

Given the potentially large number of organic species in ambient particles, bulk chemical measurements are useful to describe the extent of oxidative aging of SOA. Using aerosol mass spectrometry, changes in O:C (elemental oxygen to carbon ratio) and H:C (elemental hydrogen to carbon ratio) from high-resolution data and f_{44} (ratio of mass-to-charge (m/z) 44 to total signal in the organic component mass spectrum) and f_{43} (ratio of m/z 43 to total signal in the organic component mass spectrum) have been reported for ambient and laboratory-generated particles. The dominant organic ion at m/z 43 is $C_2H_3O^+$, and the dominant organic ion at m/z 44 is CO_2^+ . Ng et al. (2010) evaluated a number of aerosol oxidation data sets in the $f_{44} - f_{43}$ space and found that data for ambient OA tend to occupy a triangular region. As the OA becomes more

Title Page

Abstract

Introduction

Conclusions

References

Tables

Figures

◀

▶

◀

▶

Back

Close

Full Screen / Esc

Printer-friendly Version

Interactive Discussion



***m*-Xylene SOA aging**

C. L. Loza et al.

[Title Page](#)[Abstract](#)[Introduction](#)[Conclusions](#)[References](#)[Tables](#)[Figures](#)[◀](#)[▶](#)[◀](#)[▶](#)[Back](#)[Close](#)[Full Screen / Esc](#)[Printer-friendly Version](#)[Interactive Discussion](#)

oxidized, it tends to move from a region of lower f_{44} and a wider range of f_{43} at the base of the triangle toward the apex with higher f_{44} and less variable f_{43} . Heald et al. (2010) used the Van Krevelen diagram to show that data on the H:C and O:C of total ambient OA tend to fall along a line with a slope of -1 , suggesting, on average, equal additions of carbonyl and alcohol moieties. More recently, Ng et al. (2011) determined a correlation between f_{43} and H:C and, combined with a correlation between f_{44} and O:C (Aiken et al., 2008), mapped the triangular region in $f_{44} - f_{43}$ space onto the Van Krevelen diagram. They found that for ambient OA classified as oxygenated OA (OOA) and laboratory chamber-generated SOA the H:C and O:C evolution toward the apex of the triangle tends to fall along a line with a slope of -0.5 on a Van Krevelen diagram. This difference in slope between the two studies was attributed to the inclusion of primary OA in the study of Heald et al. The evolution of ambient OA can also be represented in terms of saturation concentration (C^*) and O:C (Jimenez et al., 2009). As the OA becomes more oxidized, C^* decreases and O:C increases. In all three of these frameworks, the oxygen content of the organic aerosol increases upon aging.

Laboratory studies have been conducted to probe the mechanisms of chemical aging of SOA. In flow reactor experiments, which have much shorter residence times than chamber experiments, OH concentrations a few orders of magnitude higher than ambient concentrations are used to attain OH exposure similar to that of multiple days of atmospheric processing. Using a flow reactor, Kroll et al. (2009) found that for oxidation of squalane ($C_{30}H_{36}$) particles, functionalization reactions (addition of polar functional groups) dominated at low OH exposure, and fragmentation reactions (scission of C-C bonds in the carbon skeleton) dominated as OH exposure increased. They observed an O:C ratio of 0.45 after 35.8 squalane OH oxidation lifetimes. Lambe et al. (2011) also used a flow reactor to attain OH exposures equivalent to 1–20 days of atmospheric aging. Using a range of anthropogenic and biogenic SOA and oxidized primary organic aerosol (OPOA) precursors, they found that as OH exposure increased, the SOA and OPOA followed and extended the progression of ambient SOA in $f_{44} - f_{43}$ space, attaining values of f_{44} higher than ambient SOA. The Van Krevelen diagram slope of the

***m*-Xylene SOA aging**

C. L. Loza et al.

Title Page

Abstract

Introduction

Conclusions

References

Tables

Figures

◀

▶

◀

▶

Back

Close

Full Screen / Esc

Printer-friendly Version

Interactive Discussion



SOA and OPOA was indicative of carboxylic acid formation and carbon-carbon bond fragmentation. In chamber experiments of 16 h oxidant exposure, Qi et al. (2010) found that, starting after 2 h of OH exposure, the volatility of SOA generated from *m*-xylene and α -pinene under high-NO_x conditions decreased slowly for the remainder of the experiment. After this initial 2-h period the O:C ratio for *m*-xylene SOA increased at a rate of 0.007 h⁻¹; however, for α -pinene SOA, the O:C ratio decreased at a rate of 0.003 h⁻¹. Chhabra et al. (2010) observed increasing O:C for SOA formed from toluene, *m*-xylene, and naphthalene for irradiation times up to 12 h. The most rapid increase in O:C occurred during the first hour of low-NO_x toluene and *m*-xylene experiments and the first 4 h of low-NO_x naphthalene experiments. Similarly to the results of Qi et al. (2010) that SOA from some precursors exhibits minute aging behavior, no change in O:C was observed for SOA from isoprene photooxidation or α -pinene ozonolysis after initial SOA formation. Chhabra et al. (2011) extended the analysis of the SOA formed from the compounds studied in Chhabra et al. (2010) to assess their behavior in both $f_{44} - f_{43}$ space and Van Krevelen diagram representations. Although the SOA formed from the various precursors occupied different regions in each representation, most systems exhibited a progression similar to aging of ambient SOA.

In this work, we develop and apply to *m*-xylene SOA a procedure to extend to 36 h the experimental duration of a laboratory chamber operated as a batch reactor. Aromatic hydrocarbon emissions are an important contribution (~20–30%) to the total volatile organic compounds in the urban atmosphere (Calvert et al., 2002). *m*-Xylene SOA yields (ratio of mass concentration of SOA formed to mass concentration of parent hydrocarbon reacted) have been measured previously for *m*-xylene concentrations of 10 to 180 ppb and experimental durations up to 10 h (Ng et al., 2007; Song et al., 2007). SOA yields for low-NO_x conditions were found to be higher than those for high-NO_x conditions. In addition, Chhabra et al. (2010) and Qi et al. (2010) observed changes in SOA chemical composition for up to 16 h of oxidation, indicating the potential of aging of *m*-xylene SOA over longer timescales. For a long duration experiment, the initial *m*-xylene concentration can be chosen to produce a sufficient amount of SOA

to sample for the duration of the experiment yet remaining close to atmospherically relevant loadings, typically $0.1\text{--}20\ \mu\text{g m}^{-3}$ (Shilling et al., 2009). In the present work, the total amount of SOA formed, its chemical composition, and the composition of the gas phase over 36 h of irradiation are evaluated to infer mechanisms of chemical aging of *m*-xylene SOA.

2 Materials and methods

2.1 Experimental setup

Experiments were conducted in the Caltech dual 28-m³ Teflon chambers. Details of the facilities are given elsewhere (Cocker et al., 2001; Keywood et al., 2004). Before each experiment, the chambers were flushed with dried, purified air for > 24 h, until the particle number concentration $< 50\ \text{cm}^{-3}$ and the volume concentration $< 0.1\ \mu\text{m}^3\ \text{cm}^{-3}$. Experiments were run under low-NO_x conditions using hydrogen peroxide (H₂O₂) as the OH source. With H₂O₂ it is possible to achieve a constant OH concentration for the duration of the experiments. H₂O₂ was injected into the chamber by evaporating 280 μl of 50 % wt aqueous solution into the chamber with 5 l min⁻¹ of purified air. Seed particles were injected by atomizing a 0.015 M aqueous ammonium sulfate (AS) solution for neutral seed and a 0.03 M aqueous magnesium sulfate with 0.03 M sulfuric acid (MS + SA) solution for acidic seed. *m*-Xylene (Sigma Aldrich, 99+ %) was introduced into the chamber by injecting the volume of the liquid hydrocarbon required to obtain a concentration of 30 ppb into a glass bulb, and the vapor was carried into the chamber with 5 l min⁻¹ of purified air. The chamber contents were allowed to mix for 1 h before beginning irradiation.

A suite of instruments was used to study the evolution of the gas and particle phases. *m*-Xylene was measured using a gas chromatograph with flame ionization detector (GC/FID, Agilent 6890N), equipped with a HP-5 column (15 m × 0.53 mm ID × 1.5 μm thickness, Hewlett Packard). Reactive intermediates and H₂O₂ were continuously

[Title Page](#)[Abstract](#)[Introduction](#)[Conclusions](#)[References](#)[Tables](#)[Figures](#)[◀](#)[▶](#)[◀](#)[▶](#)[Back](#)[Close](#)[Full Screen / Esc](#)[Printer-friendly Version](#)[Interactive Discussion](#)

***m*-Xylene SOA aging**

C. L. Loza et al.

Title Page

Abstract

Introduction

Conclusions

References

Tables

Figures

◀

▶

◀

▶

Back

Close

Full Screen / Esc

Printer-friendly Version

Interactive Discussion



monitored using a custom-modified Varian 1200 triple-quadrupole chemical ionization mass spectrometer (CIMS). Details of operation can be found elsewhere (Crouse et al., 2006; Paulot et al., 2009; St. Clair et al., 2010). The CIMS was operated in negative mode in which CF_3O^- is used as the reagent ion. CF_3O^- clusters with the analyte, forming ions at m/z $\text{MW}+85$ ($\text{R}\cdot\text{CF}_3\text{O}^-$), or, with more acidic species, at m/z $\text{MW}+19$ ($\text{HF}\cdot\text{R}_{-\text{H}}^-$). Relative humidity (RH), temperature (T), NO, NO_x , and O_3 were continuously monitored. RH of the chamber was $< 5\%$. The initial chamber temperature was $\sim 19^\circ\text{C}$; however, heating from the blacklights caused a rise in temperature of approximately 5°C . NO and NO_x concentrations were below the 2 ppb detection limit of the instrument, and initial O_3 concentration was 2 ppb.

Aerosol size distribution and number concentration were measured continuously using a differential mobility analyzer (DMA, TSI, 3081) coupled to a condensation particle counter (CPC, TSI, 3760), henceforth referred to as the DMA. Real-time particle mass spectra were collected continuously by an Aerodyne High Resolution Time-of-Flight Aerosol Mass Spectrometer (DeCarlo et al., 2006; Canagaratna et al., 2007), henceforth referred to as the AMS. The AMS switched once every minute between the high resolution “W-mode” and the lower resolution, higher sensitivity “V-mode”. “V-mode” data were analyzed using a fragmentation table to separate sulfate, ammonium, and organic spectra and to time-trace specific m/z ratios. “W-mode” data were analyzed using a separate high-resolution spectra toolbox known as PIKA to determine the chemical formulas contributing to distinct m/z ratios (DeCarlo et al., 2006). The signals of organic ions below m/z 119 were used to calculate elemental ratios. The ratio of particle-phase CO^+ to CO_2^+ was approximately equal to 1, and the contribution of CO^+ to the organic signal was estimated to equal that of particle-phase CO_2^+ . The intensities of water-derived ions (H_2O^+ , OH^+ , and O^+) were estimated from particle phase CO_2^+ using the correlation suggested by Aiken et al. (2008). When comparing organic ion signals to organic and sulfate mass concentrations obtained from high-resolution data, a relative ionization intensity of 1.4 was used. AMS data reported in this work are averaged over 10-min intervals.

2.2 Aging experiment protocols

The volume of the reactor limits the duration of experiments in a chamber operated in batch mode; when sampling with all instruments, nearly half of the chamber volume is depleted in 18 h, at which point it is preferable to cease sampling due to deflation of the chamber. To achieve longer OH exposure times with all instruments sampling, sets of experiments were conducted with increasing duration and staggered instrument sampling. Instruments were grouped into two categories based upon their sampling schedule. Group I includes the AMS and a RH and T probe. Group II includes the DMA, the CIMS, the GC/FID, the O_3 analyzer, and the NO_x analyzer. All instruments were operated during initial injections before the onset of irradiation. Experimental time was considered to start at the onset of irradiation. First, two 18 h experiments were conducted with Group I and II instruments sampling for the entire duration to establish consistency in the gas and particle phases during separate experiments. Subsequent experiments of 24 h, 30 h, and 36 h were conducted to achieve longer OH exposure. The instrument sampling schedule for all experiments is given in Table 1. The entire set of 5 experiments was conducted in the same chamber to avoid any differences between chamber conditions that may arise between the dual chambers. For each of the Group II instruments, the data from all experiments were combined to track the evolution of species for the entire 36 h of OH exposure.

2.3 Total SOA formation

To determine the total SOA mass concentration in the chamber, ΔM_o , particle wall losses must be taken into account. The extent of interactions between particles deposited on the chamber walls and vapors in the chamber has not been determined completely; therefore, two limiting assumptions are used to bound this interaction. These limits were first described and applied to chamber experiments by Hildebrandt et al. (2009). In one limit, particles deposited on the wall are assumed to cease interaction with suspended vapors after deposition. In this case, the amount of organic

Title Page

Abstract

Introduction

Conclusions

References

Tables

Figures

◀

▶

◀

▶

Back

Close

Full Screen / Esc

Printer-friendly Version

Interactive Discussion



material in the deposited particles does not change after deposition, and these particles remain at the same size at which they deposited for the remainder of the experiment. In the other limit, particles on the wall are assumed to interact with vapors in the chamber after deposition as if they had remained suspended. Thus, in this case, the amount of organic material in the particles after deposition changes at the same rate as the amount of organic material in the suspended particles, and the deposited particles continue to change size throughout the remainder of the experiment. This limit is analogous in theory to that of a chamber without walls. In either limit, the material on the walls is added to that which remains suspended to obtain the total amount of SOA formed.

During particle growth, the organic mass fraction of the suspended particles increases. In the first limit, the organic mass fraction of deposited particles does not increase after deposition; therefore, this case produces a lower limit for ΔM_o . In the second limit, deposited particles are assumed to continue growing; therefore, this case is an upper limit for ΔM_o . These two limits of wall loss corrected ΔM_o will subsequently be referred to as the lower bound and upper bound, respectively.

The lower bound limit on ΔM_o is calculated from the DMA suspended particle number distribution. For each size bin i at each time step j the number distribution deposited to the wall, $n_{w,ij}$ is calculated using previously determined size-dependent wall loss rates, β_i (Keywood et al., 2004; Ng et al., 2007):

$$n_{w,ij} = n_{s,ij} \exp(\beta_i \Delta t) \quad (1)$$

where $n_{s,ij}$ is the suspended particle number distribution in size bin i at time step j , and Δt is the difference between time step j and time step $j + 1$. The deposited particle number distribution is added to the suspended particle number distribution to give a wall loss corrected number distribution, $n_{tot,ij}$, which is then converted to a volume concentration, $V_{tot,j}$, assuming spherical particles,

$$n_{tot,ij} = n_{s,ij} + n_{w,ij} \quad (2)$$

Title Page

Abstract

Introduction

Conclusions

References

Tables

Figures

◀

▶

◀

▶

Back

Close

Full Screen / Esc

Printer-friendly Version

Interactive Discussion



$$V_{\text{tot},j} = \sum_{i=1}^m \frac{n_{\text{tot},ij}}{D_{p,i} \ln 10} \times (D_{p,i+} - D_{p,i-}) \times \frac{\pi}{6} D_{p,i}^3 \quad (3)$$

where m is the total number of size bins, $D_{p,i+}$ is the upper limit diameter for size bin i , and $D_{p,i-}$ is the lower limit diameter for size bin i . A factor of $\ln 10$ is necessary to convert from a log normal distribution. The initial seed volume concentration, V_{seed} , is subtracted from the wall loss corrected volume concentration to give the volume concentration of SOA, $V_{o,j}$. To convert to SOA mass, $\Delta M_{o,j}$, the SOA volume concentration is multiplied by the SOA density, ρ_{org} ,

$$\Delta M_{o,j} = \rho_{\text{org}} (V_{o,j} - V_{\text{seed}}). \quad (4)$$

For low- NO_x m -xylene SOA, $\rho_{\text{org}} = 1.33 \text{ g cm}^{-3}$ (Ng et al., 2007).

The upper bound limit on ΔM_o is calculated by combining the AMS and DMA data. The experiments in the present work use seed particles containing sulfate, and the only process that decreases sulfate concentration in the suspended phase is wall loss. The initial sulfate concentration is calculated from the DMA seed volume concentration. There is more uncertainty for the collection efficiency of seed particles in the AMS than in the DMA. Collection efficiency in the AMS increases as organic content of the particles increases, and because the seed particles do not contain organic material, they are more susceptible to bounce in the instrument and have a collection efficiency that is less than unity (Matthew et al., 2008). To calculate the mass of sulfate in the seed, m_{SO_4} , the following equation is used:

$$m_{\text{SO}_4} = V_{\text{seed}} \rho_{\text{seed}} \frac{\text{MW}_{\text{SO}_4}}{\text{MW}_{\text{seed}}} \quad (5)$$

where ρ_{seed} is the density of the seed particles, MW_{SO_4} is the molecular weight of sulfate, and MW_{seed} is the molecular weight of the seed particles. For dry AS seed, ρ_{seed} is 1.77 g cm^{-3} . In the upper bound limit, both suspended and deposited particles gain or lose organic material at the same rate; therefore, the organic-to-sulfate ratio of

all particles is the same, and this ratio is determined from unit mass resolution AMS data. To obtain the SOA mass, the organic-to-sulfate ratio, r_{OS} , is multiplied by the initial mass of sulfate in the seed particles,

$$\Delta M_o = m_{SO_4} r_{OS}. \quad (6)$$

3 Results and discussion

3.1 SOA formation

Two experiments with the same initial conditions and 18 h of irradiation were performed to assess the reproducibility of initial conditions and SOA production (Table 2). For both AS seed and MS + SA seed, similar concentrations of *m*-xylene reacted and ΔM_o formed after 18 h of irradiation were achieved. Given the consistency between matched experiments, it was not necessary to sample for the entire duration of longer experiments. It was assumed that data collected during previous, shorter experiments are adequate to describe the same time period during longer experiments.

Figure 1 shows decay of *m*-xylene and ΔM_o corrected for wall loss for both the upper and lower bound cases over 36 h of irradiation. The lower bound ΔM_o and *m*-xylene data are a compilation of the set of AS seed experiments, but the upper bound ΔM_o data are from only the 36 h experiment because continuous data were available. The peak in SOA formation occurs before all of the *m*-xylene has been reacted. For the lower bound case, ΔM_o remains relatively stable after its peak, decreasing only slightly over 20 h of irradiation. For the upper bound case, ΔM_o peaks at approximately the same time as in the lower bound case; however, there is a pronounced decay of ΔM_o after the maximum is reached. Wall losses result in 43% of the total volume concentration of particles deposited on the wall for the lower bound case and 56% of ΔM_o deposited on the wall for the upper bound case after 36 h. The behavior of ΔM_o after peak growth will be discussed in Sect. 3.3.

Title Page

Abstract

Introduction

Conclusions

References

Tables

Figures

◀

▶

◀

▶

Back

Close

Full Screen / Esc

Printer-friendly Version

Interactive Discussion



Throughout the experiment, the OH concentration was approximately 2.5×10^6 molec. cm⁻³, as estimated from the decay of *m*-xylene and simulated by a photochemical model (see Appendix A). After 36 h of irradiation, 40 % of the initial 4 ppm of H₂O₂ injected into the chamber remained unreacted.

3.2 SOA composition

Figure 2 shows the evolution in the elemental oxygen-to-carbon ratio (O:C) of the suspended particles for all 5 of the AS seeded experiments. O:C values overlap for all of the experiments with different irradiation durations. A prominent feature of the SOA formed in this system is that SOA formed initially has an O:C ratio of 0.7. Over the first 5 h of irradiation and SOA formation, O:C decreases to 0.6. After 5 h, O:C gradually increases at a rate of 0.0012 h⁻¹ for the remainder of the irradiation period. The minimum in O:C occurs before the maximum ΔM_o is reached.

The mass spectral parameter f_{44} is commonly used to characterize SOA chemical composition. Aiken et al. (2008) determined a relationship between O:C and f_{44} for ambient aerosol in Mexico City: $O:C = (3.82 \pm 0.05) \times f_{44} + (0.0794 \pm 0.0070)$ for f_{44} ranging from 0 to 0.25. The SOA in the current set of experiments does not follow the same trend as the Mexico City SOA, and exhibits trendline of $O:C = (1.19 \pm 0.23) \times f_{44} + (0.463 \pm 0.027)$ over a range of 0.10 to 0.14 of f_{44} . Although the data for *m*-xylene SOA do not follow the same trendline as the Mexico City data, they lie within the scatter of the Mexico City data. This correlation differs from that of Lambe et al. (2011), who observed that *m*-xylene SOA follows the same trendline as the Mexico City data. The range of f_{44} values observed by Lambe et al. is much larger than that in the present work, and initial hydrocarbon loadings are higher. Either of these factors could contribute to the different correlations between O:C and f_{44} . The evolution of *m*-xylene SOA is also represented in $f_{44} - f_{43}$ space (Fig. 3). The change in O:C, derived from the correlation specific to *m*-xylene, is also shown. The marker size is a function of the concentration of suspended organics, normalized to suspended sulfate concentration to account for wall losses. Overall, low-NO_x *m*-xylene SOA exhibits higher f_{43} than

Title Page

Abstract

Introduction

Conclusions

References

Tables

Figures

◀

▶

◀

▶

Back

Close

Full Screen / Esc

Printer-friendly Version

Interactive Discussion



the typical range of ambient SOA observed by Ng et al. (2010) and lies to the right of the triangular region derived for ambient SOA. At the beginning of irradiation when the organic mass loading is small, the SOA has a higher f_{44} and a lower f_{43} . As SOA continues to form, f_{44} decreases and f_{43} increases until approximately 5 h of irradiation, at which time the trends reverse. For the remaining duration of irradiation, f_{44} increases and f_{43} decreases, resulting in a progression of the SOA characteristic of the behavior of more-aged ambient SOA. The time at which the reversal of path in $f_{44} - f_{43}$ space occurs is the same as that at which the minimum in O:C occurs.

The high-resolution AMS mass spectra provide clues to the trends in O:C, f_{44} , and f_{43} . The average mass spectra at peak organic growth and at the end of the 36-h aging experiment are shown in Fig. 4. Figure 5 shows the time trends of the 4 dominant organic ions (CH_3^+ , CHO^+ , $\text{C}_2\text{H}_3\text{O}^+$, and CO_2^+) in the aerosol mass spectra and the maximum of the suspended particle size distribution throughout 36 h of oxidation. Excluding CO_2^+ , these ions account for 30–35 % of the total organic signal throughout the experiment. When organic CO_2^+ and the ions whose organic contributions are assumed to correlate with it (CO^+ , H_2O^+ , OH^+ , and O^+) are included, the mass fraction of the organic signal is approximately 52 %. In the top panel of Fig. 5, the total amount of each of the ions in the particle mass spectra is shown. To obtain this, the ion signal was divided by the sulfate signal to correct for wall losses. The sulfate-normalized ion signal was then scaled by its average value at the peak concentration. In the middle panel, the fractional contribution of each ion to the total organic signal is shown. The bottom panel shows the particle diameter (D_p) of the maximum of the suspended particle size distribution. The most rapid change in D_p occurs during the first 5 h of irradiation. The amount of each of the 4 ions in the particles increases during this time (top panel). After 5 h, D_p changes more slowly, and the contribution of each ion to the spectra begins to peak. CHO^+ reaches a maximum most quickly, followed by CH_3^+ and $\text{C}_2\text{H}_3\text{O}^+$. CO_2^+ peaks later than the other ions. After most of the ions peak, their contribution to the spectra decreases for the remainder of the experiment; however, the amount of CO_2^+ shows much less of a decrease, suggesting that compounds that

***m*-Xylene SOA aging**

C. L. Loza et al.

Title Page

Abstract

Introduction

Conclusions

References

Tables

Figures

◀

▶

◀

▶

Back

Close

Full Screen / Esc

Printer-friendly Version

Interactive Discussion



contribute to the CO_2^+ signal have a lower tendency to be removed from the particles than those that contribute to the other ion signals.

Shortly after the onset of irradiation, CO_2^+ constitutes the largest fraction of the organic signal, likely from the condensation of low-volatility organics. As irradiation continues, the CO_2^+ fraction of the organic signal decreases as semivolatile material represented by the other ions, especially $\text{C}_2\text{H}_3\text{O}^+$, begins to partition to the particles. Once the rate of particle growth slows, the fraction of CO_2^+ increases because the contribution of CO_2^+ to the mass spectra is still increasing, whereas the amounts of the other ions are beginning to stabilize and then decrease. The increase in the organic fraction of CO_2^+ continues throughout the duration of the experiment caused by a larger decrease in the amounts of the other ions in the particle mass spectra than CO_2^+ .

3.3 Fate of SOA after peak growth

One explanation for the decrease of most of the major organic ions and the total organic mass (Fig. 1) is repartitioning of semivolatiles to the gas phase. As irradiation continues, semivolatiles in the gas phase can undergo reaction with OH or photolysis to form higher-volatility products, or they may be lost to the walls. As the concentration of a semivolatile in the gas phase decreases from fragmentation reactions or wall loss, repartitioning can occur to maintain gas-particle equilibrium. OH can also react with the particle surface, forming higher volatility fragmentation products that evaporate and decrease the particle organic mass. These processes are summarized in Fig. 6. The decrease in ΔM_0 corresponding to the upper bound wall loss correction is greater than the lower bound wall loss correction. Evaporation of semivolatiles has a greater effect on ΔM_0 in the upper bound limit because all particles are assumed to undergo gas-particle partitioning, opposed to only the suspended particles in the lower bound limit.

Semivolatile species are expected to repartition from the particle phase more easily than low volatility species. This behavior is observed with the organic ions $\text{C}_2\text{H}_3\text{O}^+$, characteristic of semivolatile oxygenated organic aerosol (SV-OOA), and

24982

Title Page

Abstract

Introduction

Conclusions

References

Tables

Figures

◀

▶

◀

▶

Back

Close

Full Screen / Esc

Printer-friendly Version

Interactive Discussion



***m*-Xylene SOA aging**

C. L. Loza et al.

[Title Page](#)[Abstract](#)[Introduction](#)[Conclusions](#)[References](#)[Tables](#)[Figures](#)[◀](#)[▶](#)[◀](#)[▶](#)[Back](#)[Close](#)[Full Screen / Esc](#)[Printer-friendly Version](#)[Interactive Discussion](#)

CO_2^+ , characteristic of low volatility oxygenated organic aerosol (LV-OOA). The amount of $\text{C}_2\text{H}_3\text{O}^+$ in the particle mass spectra increases faster than CO_2^+ and shows a much greater decrease than CO_2^+ as the experiment progresses. There is a slight decrease in CO_2^+ at longer irradiation times, and it is possible that the uptake of low volatility species is not completely irreversible, allowing for some evaporation.

Evaporation of particles is characterized by a shift of the D_p at the maximum of the size distribution to smaller size. This shift was not observed in the aging experiments, as shown in the bottom panel of Fig. 5 where D_p increased slightly after the peak organic loading was attained around 12 h. The two main processes affecting the particle size distribution in chamber experiments are gas-particle partitioning and wall loss. In the Caltech chambers, wall loss rates are at a minimum for particles of diameters between 200 and 300 nm. During the aging experiments, the D_p at the size distribution maximum is below the 200–300 nm minimum in wall loss. If evaporation is occurring, the rate of wall loss will increase as particles get smaller. As a result, the greater loss of small particles will cause the size distribution, characterized by the D_p at its maximum, to shift slightly toward the 200–300 nm minimum in wall loss rate. Both the evaporation and wall loss processes are slow; therefore, the two processes will tend to counteract each other with respect to their effects on the dynamics of the aerosol size distribution, and no change in D_p at the maximum of the size distribution is observed.

To determine the extent to which photochemical processes are affecting the aerosol after peak growth, an experiment was performed in which the lights were turned off after 12.4 h of irradiation (Fig. 7). Production of OH ceases, and shortly thereafter, OH is no longer present in the chambers. The *m*-xylene concentration stabilizes after lights are turned off, and the substantial decrease in the upper bound ΔM_o is not observed with the lights off. No decrease in ΔM_o for the lower bound limit is observed. After the lights are turned off, the chemical composition of the particles also stops changing significantly. This is shown in $f_{44} - f_{43}$ space in Fig. 8. While the aerosol forms, f_{43} decreases and f_{44} increases; however, after the lights are turned off, the rates of change of both f_{43} and f_{44} decrease substantially. In the absence of irradiation, a

semivolatile species in the gas phase, A^g , can partition to and from particles or be lost to the walls (Fig. 6). After irradiation stops, no change in the amount and composition of the particles is observed; therefore, no significant repartitioning is occurring. Under these conditions, only vapor phase wall loss is expected to cause repartitioning; therefore, vapor phase wall loss is not significant in this system. If no repartitioning is observed without irradiation, and if there are no substantial vapor phase wall losses, then repartitioning must be driven by photochemical processes that affect the chemical composition of the gases and SOA.

It was not possible to distinguish among the photochemical process occurring: reaction of OH with semivolatiles; reaction of OH with particles; and photolysis of semivolatiles. The photochemical model was used to estimate lifetimes for semivolatiles against OH reaction, particles against OH reaction, and semivolatiles against photolysis. The lifetime of OH against reaction with gas-phase species A^g , τ_{A+OH} (s), is

$$\tau_{A+OH} = \frac{1}{k_{A+OH}c_A} \quad (7)$$

where k_{A+OH} ($\text{cm}^3 \text{ molec.}^{-1} \text{ s}^{-1}$) is the reaction rate constant and c_A (molec. cm^{-3}) is the gas-phase concentration of A. Using the combined concentrations of species ROOH, ROHOH, ROHOOH, and EPOXOOH and an average rate constant $k_{OH} = 1 \times 10^{-10} \text{ cm}^3 \text{ molec.}^{-1} \text{ s}^{-1}$, $\tau_{A+OH} \cong 0.2 \text{ s}$. Three of these species, ROOH, ROHOH, and EPOXOOH, can also undergo photolysis. The lifetime of these species against photolysis, $\tau_{A+h\nu}$, is calculated by,

$$\tau_{A+h\nu} = \frac{1}{j_{\text{ROOH}}} \quad (8)$$

where j_{ROOH} is the photolysis rate constant of an organic peroxide, as described in Appendix A. The characteristic lifetime against photolysis is estimated as $4.7 \times 10^5 \text{ s}$. The heterogeneous reaction of OH with a particle surface is assumed to be

Title Page

Abstract

Introduction

Conclusions

References

Tables

Figures

◀

▶

◀

▶

Back

Close

Full Screen / Esc

Printer-friendly Version

Interactive Discussion



pseudo-first order in terms of OH (Seinfeld and Pandis, 2006). The characteristic time for this process, τ_{P+OH} (s), can be calculated by,

$$\tau_{P+OH} = \frac{1}{\frac{1}{4}\gamma\overline{c_{OH}}A_p} \quad (9)$$

where γ is an uptake coefficient, here assumed to be 1, A_p ($\text{cm}^2 \text{cm}^{-3}$) is the surface area concentration of the particles, and $\overline{c_{OH}}$ (cm s^{-1}) is given by

$$\overline{c_{OH}} = \left(\frac{8RT}{\pi MW_{OH}} \right)^{\frac{1}{2}} \quad (10)$$

where T (K) is temperature and MW_{OH} (kg mol^{-1}) is the molecular weight of OH. Based on the upper and lower bound wall loss corrections, τ_{P+OH} ranges from 6–13.5 s. The estimated characteristic time for reaction of OH with semivolatile vapors is an order of magnitude shorter than that for OH reaction with particles, and both are considerably shorter than that for photolysis of semivolatiles; therefore, it appears that changes in particle composition are likely driven by continued oxidation of the gas phase, although OH reaction with particle surfaces cannot be categorically dismissed.

The continued oxidation of semivolatile species is apparent upon examination of possible gas-phase *m*-xylene oxidation products using the CIMS (Fig. 9). The top panel shows the time trace of *m/z* 207, which has the same *m/z* as the predicted reagent ion clustering of first-generation oxidation products ROH (MW +85) and ROOH (MW +19) in the model (Table 4). This *m/z* signal increases rapidly and peaks at 3–4 h of irradiation. When lights are turned off during the experiment, the decay slows significantly. The middle panel shows the time trace of *m/z* 223, which has the same *m/z* as the predicted reagent ion clustering of second-generation oxidation products ROHOH (MW +85), ROHOOH (MW +19), and EPOXOOH (MW +19). Again, this *m/z* signal increases rapidly and peaks slightly later at 4–5 h irradiation. When the lights are turned off, the signal stabilizes. The bottom panel shows the time trace of *m/z* 271, which

[Title Page](#)[Abstract](#)[Introduction](#)[Conclusions](#)[References](#)[Tables](#)[Figures](#)[◀](#)[▶](#)[◀](#)[▶](#)[Back](#)[Close](#)[Full Screen / Esc](#)[Printer-friendly Version](#)[Interactive Discussion](#)

has the same m/z as the predicted reagent ion clustering of third-generation oxidation product (MW +85) formed by the EPOXOOH + OH reaction ($\text{prod}_{\text{EPOXOOH}+\text{OH}}$ in the model). From model predictions, this compound with predicted reagent ion clustering at m/z 271 should form more slowly. The signal at m/z 271 peaks at 13–14 h of irradiation and does not decrease after irradiation ceases. The behavior of these signals is consistent with multiple generations of oxidation. The changes are clearly photochemically driven. Vapor-phase wall loss is not a significant sink of compounds contributing to these signals indicated by the absence of decay after the lights are turned off.

3.4 Acidic seed effects

Aging experiments were also performed using acidic MS+SA seed to determine the extent to which particle acidity affects chemical aging of *m*-xylene SOA. Figure 10 shows the elemental ratios for both AS and MS + SA seeded experiments. No difference between the acidic and neutral seeds for *m*-xylene-derived SOA is observed. Ng et al. (2007) did not observe a difference in yields for low- NO_x *m*-xylene SOA with neutral and acidic seed particles; therefore, it is plausible that the chemical composition of the aerosol condensed onto the two types of seed particles is similar.

4 Conclusions

Laboratory chamber studies provide fundamental information on the mechanisms of formation of SOA. The duration of chamber experiments is limited by several factors, including wall loss of particles and vapors and depletion of chamber air through instrument sampling. Laboratory experiments attempt to approach durations of OH radical exposure corresponding to those of particles in the atmosphere, the order of a week, through enhanced OH radical levels. In the present work we extend the duration of chamber experiments by sampling protocols that minimize the amount of chamber air removed over the course of the experiment. The protocol developed here allows

Title Page

Abstract

Introduction

Conclusions

References

Tables

Figures

◀

▶

◀

▶

Back

Close

Full Screen / Esc

Printer-friendly Version

Interactive Discussion



experiments up to 36 h duration. Hydroxyl radical levels in the experiments reported here are roughly at atmospheric levels. We address SOA formation from the photooxidation of *m*-xylene, an important anthropogenic precursor to organic aerosol. The extended duration experiments provide a view into the multi-generational chemistry involved in *m*-xylene SOA formation that can be expected to be occurring in the atmosphere. Although the current work studies only low-NO_x chemistry, the *m*-xylene oxidation mechanism leading to SOA formation under high-NO_x conditions is also expected to follow multi-generational chemistry (Kwok et al., 1997; Zhao et al., 2005; Ng et al., 2007; Song et al., 2007; Noda et al., 2009; Birdsall et al., 2010). The generations of oxidation of a precursor volatile organic compound can lead to functionalized products of ever decreasing volatility, characterized by increasing elemental O:C ratio, as well as to products of higher volatility that do not contribute to SOA. The evolution of the O:C ratio in the *m*-xylene system exhibits behavior characteristic of gas-particle partitioning in which initially only highly oxidized products condense when the overall aerosol loading is small, followed by a decrease in O:C ratio as products of somewhat higher volatility condense into the growing amount of aerosol. As the gas-phase oxidation progresses through higher generations, products of higher oxidation state are generated and condense; however, the continued oxidation can also lead to fragmentation reactions forming products of higher volatility that do not condense. Based on CIMS measurements, there is strong evidence of gas-phase loss of higher generation products. That this process involves photooxidation or photolysis is confirmed by the absence of changes in total aerosol amount when irradiation is stopped. Wall loss of vapor can be excluded as the cause of this behavior. Estimates of reaction timescales suggest that gas-phase processes are most likely involved in this latter stage of aging, although direct OH reaction with the surface of the particles cannot be ruled out. Finally, the present work offers a protocol for laboratory chamber experiments to attain times approaching more closely those of atmospheric aerosol residence times.

***m*-Xylene SOA aging**

C. L. Loza et al.

Title Page

Abstract

Introduction

Conclusions

References

Tables

Figures

◀

▶

◀

▶

Back

Close

Full Screen / Esc

Printer-friendly Version

Interactive Discussion



Photochemical model

To estimate both OH concentration and the importance of OH reaction with later-generation oxidation products, a photochemical model (Reactions R1–R23 below) was constructed. Products through three generations of oxidation are included. Primary oxidation products are those suggested by Birdsall et al. (2010) and Zhao et al. (2005) with product yields and further oxidative pathways as derived from the MCM (Jenkin et al., 2003; Bloss et al., 2005). Values of rate constants are listed in Table 3, and compounds represented in the model are given in Table 4. Photolysis rate constants are calculated using the irradiance spectrum measured for the chamber lights and absorption cross section values and quantum yields from Sander et al. (2011). The following reactions are included:

*m*-Xylene SOA aging

C. L. Loza et al.

Title Page

Abstract

Introduction

Conclusions

References

Tables

Figures

◀

▶

◀

▶

Back

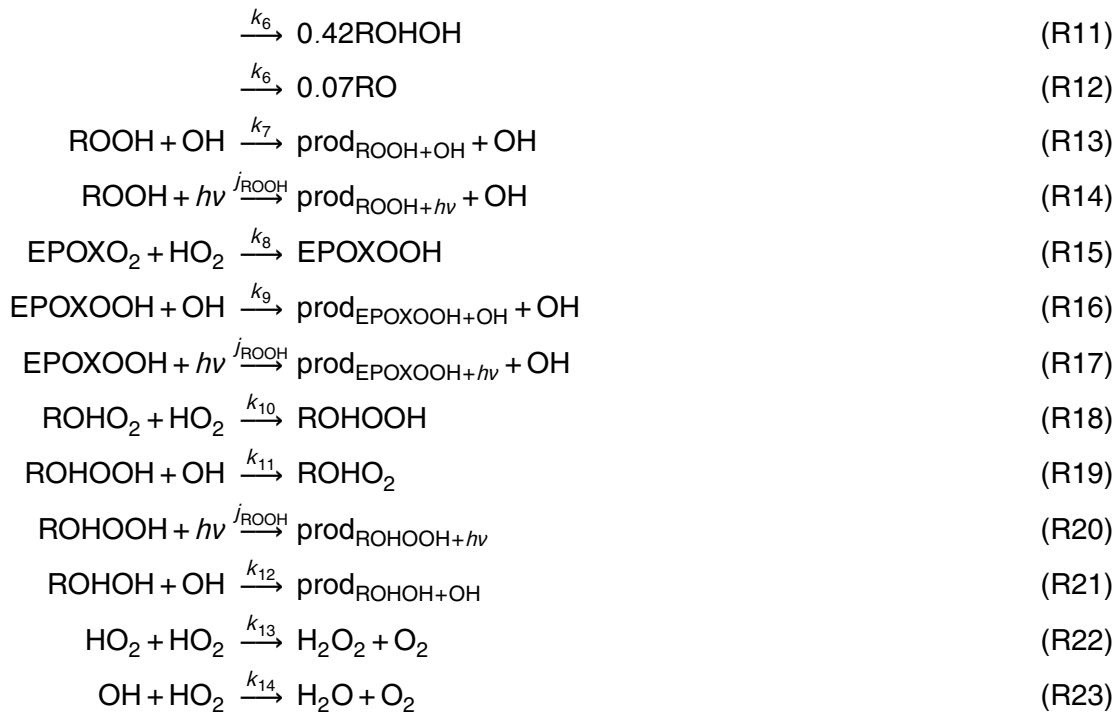
Close

Full Screen / Esc

Printer-friendly Version

Interactive Discussion





Acknowledgements. This work was supported by the Office of Science (Biological and Environmental Research), US Department of Energy, and National Science Foundation Grant AGS-1057183. The CIMS instrument was purchased as part of a major research instrumentation grant from the National Science Foundation (Grant ATM-0619783); assembly and testing was supported by the Davidow Discovery Fund. We thank Katherine A. Schilling and ManNin Chan for experimental assistance and Arthur W. H. Chan for helpful discussion. Christine Loza, Lindsay Yee, and Jill Craven were supported by National Science Foundation Graduate Research Fellowships.

Title Page

Abstract

Introduction

Conclusions

References

Tables

Figures

◀

▶

◀

▶

Back

Close

Full Screen / Esc

Printer-friendly Version

Interactive Discussion



References

- Aiken, A. C., DeCarlo, P. F., Kroll, J. H., Worsnop, D. R., Huffman, J. A., Docherty, K. S., Ulbrich, I. M., Mohr, C., Kimmel, J. R., Sueper, D., Sun, Y., Zhang, Q., Trimborn, A., Northway, M., Ziemann, P. J., Canagaratna, M. R., Onasch, T. B., Alfarra, M. R., Prevot, A. S. H., Dommen, J., Duplissy, J., Metzger, A., Baltensperger, U., and Jimenez, J. L.: O/C and OM/OC ratios of primary, secondary, and ambient organic aerosols with high-resolution time-of-flight aerosol mass spectrometry, *Environ. Sci. Technol.*, 42, 4478–4485, doi:10.1021/es703009q, 2008. 24972, 24975, 24980
- Balkanski, Y. J., Jacob, D. J., D. J., Gardner, G. M., Graustein, W. C., and Turekian, K. K.: Transport and residence times of tropospheric aerosols inferred from a global 3-dimensional simulation of PB-210, *J. Geophys. Res.-Atmos.*, 98, 20573–20586, doi:10.1029/93JD02456, 1993. 24971
- Birdsall, A. W., Andreoni, J. F., and Elrod, M. J.: Investigation of the role of bicyclic peroxy radicals in the oxidation mechanism of toluene, *J. Phys. Chem. A*, 114, 10655–10663, doi:10.1021/jp105467e, 2010. 24987, 24988, 24998
- Bloss, C., Wagner, V., Jenkin, M. E., Volkamer, R., Bloss, W. J., Lee, J. D., Heard, D. E., Wirtz, K., Martin-Reviejo, M., Rea, G., Wenger, J. C., and Pilling, M. J.: Development of a detailed chemical mechanism (MCMv3.1) for the atmospheric oxidation of aromatic hydrocarbons, *Atmos. Chem. Phys.*, 5, 641–664, doi:10.5194/acp-5-641-2005, 2005. 24988, 24998
- Calvert, J. G., Atkinson, R., H., B. K., Kamens, R. M., Seinfeld, J. H., Wallington, T. J., and Yarwood, G.: *The Mechanisms of Atmospheric Oxidation of Aromatic Hydrocarbons*, Oxford University Press, New York, 2002. 24973, 24998
- Canagaratna, M. R., Jayne, J. T., Jimenez, J. L., Allan, J. D., Alfarra, M. R., Zhang, Q., Onasch, T. B., Drewnick, F., Coe, H., Middlebrook, A., Delia, A., Williams, L. R., Trimborn, A. M., Northway, M. J., DeCarlo, P. F., Kolb, C. E., Davidovits, P., and Worsnop, D. R.: Chemical and microphysical characterization of ambient aerosols with the Aerodyne aerosol mass spectrometer, *Mass Spectrom. Rev.*, 26, 185–222, doi:10.1002/mas.20115, 2007. 24975
- Chhabra, P. S., Flagan, R. C., and Seinfeld, J. H.: Elemental analysis of chamber organic aerosol using an aerodyne high-resolution aerosol mass spectrometer, *Atmos. Chem. Phys.*, 10, 4111–4131, doi:10.5194/acp-10-4111-2010, 2010. 24973
- Chhabra, P. S., Ng, N. L., Canagaratna, M. R., Corrigan, A. L., Russell, L. M., Worsnop, D. R., Flagan, R. C., and Seinfeld, J. H.: Elemental composition and oxidation of chamber organic

Title Page

Abstract

Introduction

Conclusions

References

Tables

Figures

◀

▶

◀

▶

Back

Close

Full Screen / Esc

Printer-friendly Version

Interactive Discussion



***m*-Xylene SOA aging**

C. L. Loza et al.

Title Page

Abstract

Introduction

Conclusions

References

Tables

Figures

◀

▶

◀

▶

Back

Close

Full Screen / Esc

Printer-friendly Version

Interactive Discussion



- aerosol, *Atmos. Chem. Phys.*, 11, 8827–8845, doi:10.5194/acp-11-8827-2011, 2011. 24973
- Cocker, D. R., Flagan, R. C., and Seinfeld, J. H.: State-of-the-art chamber facility for studying atmospheric aerosol chemistry, *Environ. Sci. Technol.*, 35, 2594–2601, doi:10.1021/es0019169, 2001. 24974
- 5 Crounse, J. D., McKinney, K. A., Kwan, A. J., and Wennberg, P. O.: Measurement of gas-phase hydroperoxides by chemical ionization mass spectrometry, *Anal. Chem.*, 78, 6726–6732, doi:10.1021/ac0604235, 2006. 24975
- DeCarlo, P. F., Kimmel, J. R., Trimborn, A., Northway, M. J., Jayne, J. T., Aiken, A. C., Gonin, M., Fuhrer, K., Horvath, T., Docherty, K. S., Worsnop, D. R., and Jimenez, J. L.: Field-deployable, high-resolution, time-of-flight aerosol mass spectrometer, *Anal. Chem.*, 78, 8281–8289, doi:10.1021/ac061249n, 2006. 24975
- 10 Hallquist, M., Wenger, J. C., Baltensperger, U., Rudich, Y., Simpson, D., Claeys, M., Dommen, J., Donahue, N. M., George, C., Goldstein, A. H., Hamilton, J. F., Herrmann, H., Hoffmann, T., Iinuma, Y., Jang, M., Jenkin, M. E., Jimenez, J. L., Kiendler-Scharr, A., Maenhaut, W., McFiggans, G., Mentel, Th. F., Monod, A., Prévôt, A. S. H., Seinfeld, J. H., Surratt, J. D., Szmigielski, R., and Wildt, J.: The formation, properties and impact of secondary organic aerosol: current and emerging issues, *Atmos. Chem. Phys.*, 9, 5155–5236, doi:10.5194/acp-9-5155-2009, 2009. 24971
- 15 Heald, C. L., Kroll, J. H., Jimenez, J. L., Docherty, K. S., DeCarlo, P. F., Aiken, A. C., Chen, Q., Martin, S. T., Farmer, D. K., and Artaxo, P.: A simplified description of the evolution of organic aerosol composition in the atmosphere, *Geophys. Res. Lett.*, 37, L08803, doi:10.1029/2010GL042737, 2010. 24972
- Hildebrandt, L., Donahue, N. M., and Pandis, S. N.: High formation of secondary organic aerosol from the photo-oxidation of toluene, *Atmos. Chem. Phys.*, 9, 2973–2986, doi:10.5194/acp-9-2973-2009, 2009. 24976
- 25 Jenkin, M. E., Saunders, S. M., Wagner, V., and Pilling, M. J.: Protocol for the development of the Master Chemical Mechanism, MCM v3 (Part B): tropospheric degradation of aromatic volatile organic compounds, *Atmos. Chem. Phys.*, 3, 181–193, doi:10.5194/acp-3-181-2003, 2003. 24988, 24998
- 30 Jimenez, J. L., Canagaratna, M. R., Donahue, N. M., Prevot, A. S. H., Zhang, Q., Kroll, J. H., DeCarlo, P. F., Allan, J. D., Coe, H., Ng, N. L., Aiken, A. C., Docherty, K. S., Ulbrich, I. M., Grieshop, A. P., Robinson, A. L., Duplissy, J., Smith, J. D., Wilson, K. R., Lanz, V. A., Hueglin, C., Sun, Y. L., Tian, J., Laaksonen, A., Raatikainen, T., Rautiainen, J., Vaattovaara, P., Ehn,

***m*-Xylene SOA aging**

C. L. Loza et al.

Title Page

Abstract

Introduction

Conclusions

References

Tables

Figures

◀

▶

◀

▶

Back

Close

Full Screen / Esc

Printer-friendly Version

Interactive Discussion



M., Kulmala, M., Tomlinson, J. M., Collins, D. R., Cubison, M. J., Dunlea, E. J., Huffman, J. A., Onasch, T. B., Alfarra, M. R., Williams, P. I., Bower, K., Kondo, Y., Schneider, J., Drewnick, F., Borrmann, S., Weimer, S., Demerjian, K., Salcedo, D., Cottrell, L., Griffin, R., Takami, A., Miyoshi, T., Hatakeyama, S., Shimono, A., Sun, J. Y., Zhang, Y. M., Dzepina, K., Kimmel, J. R., Sueper, D., Jayne, J. T., Herndon, S. C., Trimborn, A. M., Williams, L. R., Wood, E. C., Middlebrook, A. M., Kolb, C. E., Baltensperger, U., and Worsnop, D. R.: Evolution of organic aerosols in the atmosphere, *Science*, 326, 1525–1529, doi:10.1126/science.1180353, 2009. 24972

Keywood, M. D., Varutbangkul, V., Bahreini, R., Flagan, R. C., and Seinfeld, J. H.: Secondary organic aerosol formation from the ozonolysis of cycloalkenes and related compounds, *Environ. Sci. Technol.*, 38, 4157–4164, doi:10.1021/es035363o, 2004. 24974, 24977

Kroll, J. and Seinfeld, J.: Chemistry of secondary organic aerosol: Formation and evolution of low-volatility organics in the atmosphere, *Atmos. Environ.*, 42, 3593–3624, doi:10.1016/j.atmosenv.2008.01.003, 2008. 24971

Kroll, J. H., Smith, J. D., Che, D. L., Kessler, S. H., Worsnop, D. R., and Wilson, K. R.: Measurement of fragmentation and functionalization pathways in the heterogeneous oxidation of oxidized organic aerosol, *Phys. Chem. Chem. Phys.*, 11, 8005–8014, doi:10.1039/b905289e, 2009. 24972

Kwok, E., Aschmann, S., Atkinson, R., and Arey, J.: Products of the gas-phase reactions of *o*-, *m*- and *p*-xylene with the OH radical in the presence and absence of NO_x, *J. Chem. Soc., Faraday Trans.*, 93, 2847–2854, 1997. 24987

Lambe, A. T., Onasch, T. B., Massoli, P., Croasdale, D. R., Wright, J. P., Ahern, A. T., Williams, L. R., Worsnop, D. R., Brune, W. H., and Davidovits, P.: Laboratory studies of the chemical composition and cloud condensation nuclei (CCN) activity of secondary organic aerosol (SOA) and oxidized primary organic aerosol (OPOA), *Atmos. Chem. Phys.*, 11, 8913–8928, doi:10.5194/acp-11-8913-2011, 2011. 24972, 24980

Matthew, B. M., Middlebrook, A. M., and Onasch, T. B.: Collection efficiencies in an Aerodyne aerosol mass spectrometer as a function of particle phase for laboratory generated aerosols, *Aerosol Sci. Tech.*, 42, 884–898, doi:10.1080/02786820802356797, 2008. 24978

Murphy, D. M., Cziczo, D. J., Froyd, K. D., Hudson, P. K., Matthew, B. M., Middlebrook, A. M., Peltier, R. E., Sullivan, A., Thomson, D. S., and Weber, R. J.: Single-particle mass spectrometry of tropospheric aerosol particles, *J. Geophys. Res.-Atmos.*, 111, doi:10.1029/2006JD007340, 2006. 24971

***m*-Xylene SOA aging**

C. L. Loza et al.

Title Page

Abstract

Introduction

Conclusions

References

Tables

Figures

◀

▶

◀

▶

Back

Close

Full Screen / Esc

Printer-friendly Version

Interactive Discussion



- Ng, N. L., Chhabra, P. S., Chan, A. W. H., Surratt, J. D., Kroll, J. H., Kwan, A. J., McCabe, D. C., Wennberg, P. O., Sorooshian, A., Murphy, S. M., Dalleska, N. F., Flagan, R. C., and Seinfeld, J. H.: Effect of NO_x level on secondary organic aerosol (SOA) formation from the photooxidation of terpenes, *Atmos. Chem. Phys.*, 7, 5159–5174, doi:10.5194/acp-7-5159-2007, 2007. 24973, 24977, 24978, 24986, 24987
- 5 Ng, N. L., Canagaratna, M. R., Zhang, Q., Jimenez, J. L., Tian, J., Ulbrich, I. M., Kroll, J. H., Docherty, K. S., Chhabra, P. S., Bahreini, R., Murphy, S. M., Seinfeld, J. H., Hildebrandt, L., Donahue, N. M., DeCarlo, P. F., Lanz, V. A., Prévôt, A. S. H., Dinar, E., Rudich, Y., and Worsnop, D. R.: Organic aerosol components observed in Northern Hemispheric datasets from Aerosol Mass Spectrometry, *Atmos. Chem. Phys.*, 10, 4625–4641, doi:10.5194/acp-10-4625-2010, 2010. 24971, 24981, 25003, 25008
- 10 Ng, N. L., Canagaratna, M. R., Jimenez, J. L., Chhabra, P. S., Seinfeld, J. H., and Worsnop, D. R.: Changes in organic aerosol composition with aging inferred from aerosol mass spectra, *Aerosol Sci. Tech.*, 11, 6465–6474, doi:10.5194/acp-11-6465-2011, 2011. 24972
- 15 Noda, J., Volkamer, R., and Molina, M. J.: Dealkylation of alkylbenzenes: a significant pathway in the toluene, *o*-, *m*-, *p*-xylene + OH reaction, *J. Phys. Chem. A*, 113, 9658–9666, doi:10.1021/jp901529k, 2009. 24987
- Paulot, F., Crounse, J. D., Kjaergaard, H. G., Kurten, A., St Clair, J. M., Seinfeld, J. H., and Wennberg, P. O.: Unexpected epoxide formation in the gas-phase photooxidation of isoprene, *Science*, 325, 730–733, doi:10.1126/science.1172910, 2009. 24975
- 20 Qi, L., Nakao, S., Malloy, Q., Warren, B., and Cocker, D. R.: Can secondary organic aerosol formed in an atmospheric simulation chamber continuously age?, *Atmos. Environ.*, 44, 2990–2996, doi:10.1016/j.atmosenv.2010.05.020, 2010. 24973
- Rudich, Y., Donahue, N. M., and Mentel, T. F.: Aging of organic aerosol: Bridging the gap between laboratory and field studies, *Annu. Rev. Phys. Chem.*, 58, 321–352, doi:10.1146/annurev.physchem.58.032806.104432, 2007. 24971
- 25 Sander, S. P., Abbatt, J., Barker, J. R., Burkholder, J. B., Friedl, R. R., Golden, D. M., Huie, R. E., Kolb, C. E., J., K. M., Moortgat, G. K., Orkin, V. L., and Wine, P. H.: Chemical kinetics and photochemical data for use in atmospheric studies, Evaluation No. 17. JPL Publication 10-6, Jet Propulsion Laboratory, Pasadena, <http://jpldataeval.jpl.nasa.gov>, 2011. 24988, 24998
- 30 Seinfeld, J. H. and Pandis, S. N.: *Atmospheric Chemistry and Physics*, John Wiley and Sons, Inc., Hoboken, N.J., second edn., 2006. 24985

***m*-Xylene SOA aging**

C. L. Loza et al.

[Title Page](#)[Abstract](#)[Introduction](#)[Conclusions](#)[References](#)[Tables](#)[Figures](#)[◀](#)[▶](#)[◀](#)[▶](#)[Back](#)[Close](#)[Full Screen / Esc](#)[Printer-friendly Version](#)[Interactive Discussion](#)

- Shilling, J. E., Chen, Q., King, S. M., Rosenoern, T., Kroll, J. H., Worsnop, D. R., DeCarlo, P. F., Aiken, A. C., Sueper, D., Jimenez, J. L., and Martin, S. T.: Loading-dependent elemental composition of α -pinene SOA particles, *Atmos. Chem. Phys.*, 9, 771–782, doi:10.5194/acp-9-771-2009, 2009. 24974
- 5 Shiraiwa, M., Ammann, M., Koop, T., and Pöschl, U.: Gas uptake and chemical aging of semisolid organic aerosol particles, *P. Natl. Acad. Sci. USA*, 108, 11003–11008, doi:10.1073/pnas.1103045108, 2011. 25006
- Song, C., Na, K., Warren, B., Malloy, Q., and Cocker, D. R.: Secondary organic aerosol formation from *m*-xylene in the absence of NO_x , *Environ. Sci. Technol.*, 41, 7409–7416, doi:10.1021/es070429r, 2007. 24973, 24987
- 10 St. Clair, J. M., McCabe, D. C., Crounse, J. D., Steiner, U., and Wennberg, P. O.: Chemical ionization tandem mass spectrometer for the in situ measurement of methyl hydrogen peroxide, *Rev. Sci. Instrum.*, 81, 094102, doi:10.1063/1.3480552, 2010. 24975
- Vaden, T. D., Song, C., Zaveri, R. A., Imre, D., and Zelenyuk, A.: Morphology of mixed primary and secondary organic particles and the adsorption of spectator organic gases during aerosol formation, *P. Natl. Acad. Sci. USA*, 107, 6658–6663, doi:10.1073/pnas.0911206107, 2010. 25006
- 15 Vaden, T. D., Imre, D., Beránek, J., Shrivastava, M., and Zelenyuk, A.: Evaporation kinetics and phase of laboratory and ambient secondary organic aerosol, *P. Natl. Acad. Sci. USA*, 108, 2190–2195, doi:10.1073/pnas.1013391108, 2011. 25006
- Virtanen, A., Joutsensaari, J., Koop, T., Kannosto, J., Yli-Pirilä, P., Leskinen, J., Mäkelä, J. M., Holopainen, J. K., Pöschl, U., Kulmala, M., Worsnop, D. R., and Laaksonen, A.: An amorphous solid state of biogenic secondary organic aerosol particles, *Nature*, 467, 824–827, doi:10.1038/nature09455, 2010. 25006
- 25 Zhang, Q., Jimenez, J. L., Canagaratna, M. R., Allan, J. D., Coe, H., Ulbrich, I., Alfarra, M. R., Takami, A., Middlebrook, A. M., Sun, Y. L., Dzepina, K., Dunlea, E., Docherty, K., DeCarlo, P. F., Salcedo, D., Onasch, T., Jayne, J. T., Miyoshi, T., Shimonono, A., Hatakeyama, S., Takegawa, N., Kondo, Y., Schneider, J., Drewnick, F., Borrmann, S., Weimer, S., Demerjian, K., Williams, P., Bower, K., Bahreini, R., Cottrell, L., Griffin, R. J., Rautiainen, J., Sun, J. Y., Zhang, Y. M., and Worsnop, D. R.: Ubiquity and dominance of oxygenated species in organic aerosols in anthropogenically-influenced Northern Hemisphere midlatitudes, *Geophys. Res. Lett.*, 34, L13801, doi:10.1029/2007GL029979, 2007. 24971
- 30

Zhao, J., Zhang, R., Misawa, K., and Shibuya, K.: Experimental product study of the OH-initiated oxidation of *m*-xylene, *J. Photoch. Photobio. A*, 176, 199–207, doi:10.1016/j.jphotochem.2005.07.013, 2005. 24987, 24988

***m*-Xylene SOA aging**

C. L. Loza et al.

Title Page

Abstract

Introduction

Conclusions

References

Tables

Figures



Back

Close

Full Screen / Esc

Printer-friendly Version

Interactive Discussion



***m*-Xylene SOA aging**

C. L. Loza et al.

Title Page

Abstract

Introduction

Conclusions

References

Tables

Figures

I◀

▶I

◀

▶

Back

Close

Full Screen / Esc

Printer-friendly Version

Interactive Discussion

**Table 1.** Instrument sampling protocol (times reported in elapsed hours).

Group	Experiment duration			
	18 h	24 h	30 h	36 h
I ^a	0–18	0–24	0–30	0–36
II ^a	0–18	16–24	22–30	28–36

^a Group I instruments are the AMS and a RH and *T* probe.

^b Group II instruments are the DMA, CIMS, GC/FID, O₃ analyzer, and NO_x analyzer.

***m*-Xylene SOA aging**

C. L. Loza et al.

Title Page

Abstract

Introduction

Conclusions

References

Tables

Figures

◀

▶

◀

▶

Back

Close

Full Screen / Esc

Printer-friendly Version

Interactive Discussion

**Table 2.** Experimental conditions for 18-h irradiation experiments.

Seed	Initial <i>m</i> -xylene (ppb)	Seed vol. ($\mu\text{m}^3 \text{cm}^{-3}$)	Final <i>m</i> -xylene (ppb)	Final ΔM_o^a (μgm^{-3})
AS	32.2 ± 0.7	11.1 ± 0.3	2.46 ± 0.66	21.9 ± 1.7
AS	31.8 ± 0.7	12.3 ± 0.3	0.84 ± 0.66	24.7 ± 1.9
MS+SA	32.9 ± 0.7	10.5 ± 0.4	1.94 ± 0.66	22.5 ± 1.8
MS+SA	32.4 ± 0.7	10.8 ± 0.4	1.15 ± 0.66	21.7 ± 1.7

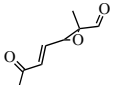
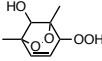
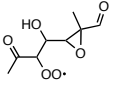
^a Lower bound limit

Table 3. Rate constants for the photochemical model.

Rate constant (cm ³ molec. ⁻¹ s ⁻¹)	Source
$j_{\text{H}_2\text{O}_2} = 2.9 \times 10^{-6}$ (s ⁻¹)	Sander et al. (2011)
$k_1 = 1.8 \times 10^{-12}$	Sander et al. (2011)
$k_2 = 2.31 \times 10^{-11}$	Calvert et al. (2002)
$k_3 = 9.8 \times 10^{-13}$	Birdsall et al. (2010)
$k_4 = 1.96 \times 10^{-11}$	MCM (Jenkin et al., 2003; Bloss et al., 2005)
$k_5 = 8.02 \times 10^{-11}$	MCM
$j_{\text{EPOX}} = 1.24 \times 10^{-4}$ (s ⁻¹)	MCM and Sander et al. (2011)
$k_6 = 9.1 \times 10^{-11}$	MCM
$k_7 = 1.17 \times 10^{-10}$	MCM
$j_{\text{ROOH}} = 2.1 \times 10^{-6}$ (s ⁻¹)	Sander et al. (2011)
$k_8 = 1.96 \times 10^{-11}$	MCM
$k_9 = 7.41 \times 10^{-11}$	MCM
$k_{10} = 1.96 \times 10^{-11}$	MCM
$k_{11} = 1.13 \times 10^{-10}$	MCM
$k_{12} = 2.05 \times 10^{-10}$	MCM
$k_{13} = 1.4 \times 10^{-12}$	Sander et al. (2011)
$k_{14} = 1.1 \times 10^{-10}$	Sander et al. (2011)

[Title Page](#)[Abstract](#)[Introduction](#)[Conclusions](#)[References](#)[Tables](#)[Figures](#)[◀](#)[▶](#)[◀](#)[▶](#)[Back](#)[Close](#)[Full Screen / Esc](#)[Printer-friendly Version](#)[Interactive Discussion](#)

Table 4. Compounds represented in the photochemical model.

Compound	Structure	Formula
RH		C_8H_{12}
RO ₂		$C_8H_{11}O_5$
EPOX		$C_8H_{10}O_3$
ROH		$C_8H_{10}O$
ROOH		$C_8H_{12}O_5$
EPOXO ₂		$C_8H_{11}O_6$
ROHO ₂		$C_8H_{11}O_6$
ROHOH		$C_8H_{10}O_2$

Title Page

Abstract

Introduction

Conclusions

References

Tables

Figures

◀

▶

◀

▶

Back

Close

Full Screen / Esc

Printer-friendly Version

Interactive Discussion



***m*-Xylene SOA aging**

C. L. Loza et al.

Title Page

Abstract

Introduction

Conclusions

References

Tables

Figures

◀

▶

◀

▶

Back

Close

Full Screen / Esc

Printer-friendly Version

Interactive Discussion

**Table 4.** Continued.

Compound	Structure	Formula
RO		C_8H_9O
EPOXOOH		$C_8H_{12}O_6$
ROHOOH		$C_8H_{12}O_6$
prod _{EPOXOOH+OH}	e.g.	$C_8H_{12}O_5$

***m*-Xylene SOA aging**

C. L. Loza et al.

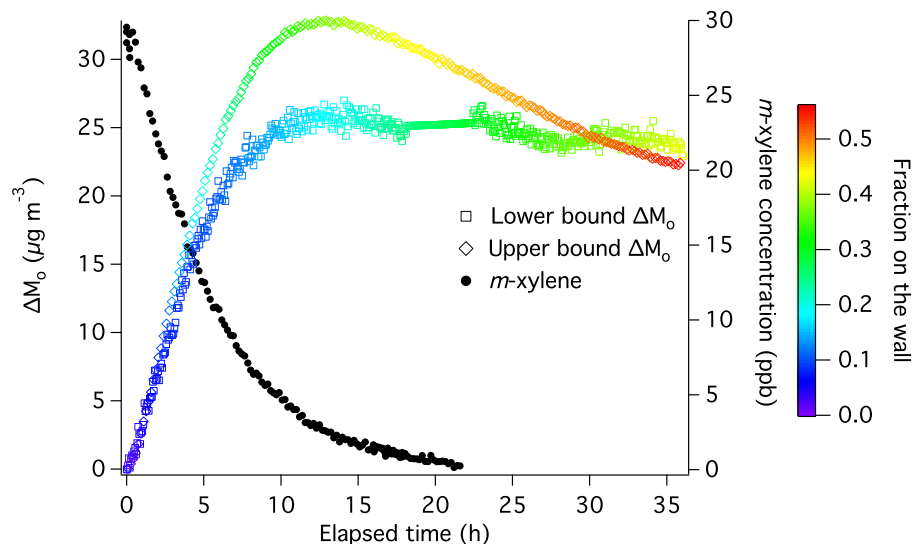


Fig. 1. SOA mass (left axis), corrected for particle wall losses, and *m*-xylene (right axis) for 36 h of OH exposure using AS seed. The lower bound ΔM_0 is calculated assuming that, once deposited, particles on the walls do not interact with gases in the chamber. The upper bound ΔM_0 assumes that, once deposited, particles continue to exhibit the same gas-particle partitioning behavior as suspended particles. The fraction on the wall for the lower bound is the ratio of particle volume on the wall to total particle volume, both suspended and deposited, and includes seed volume. The fraction on the wall for the upper bound is the ratio of organic mass concentration on the wall to the total organic mass concentration.

Title Page

Abstract

Introduction

Conclusions

References

Tables

Figures

◀

▶

◀

▶

Back

Close

Full Screen / Esc

Printer-friendly Version

Interactive Discussion



m-Xylene SOA aging

C. L. Loza et al.

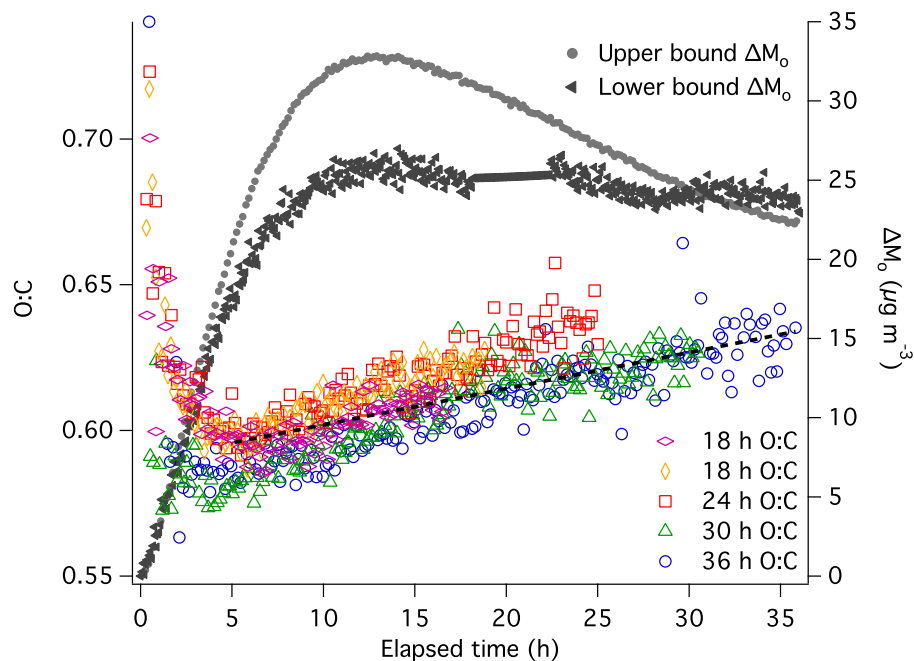


Fig. 2. SOA mass (right axis) and O:C elemental composition (left axis) over 36 h of OH exposure using AS seed. After hour 5, the O:C increases at a rate of 0.0012 h^{-1} (dashed line).

Title Page

Abstract

Introduction

Conclusions

References

Tables

Figures

◀

▶

◀

▶

Back

Close

Full Screen / Esc

Printer-friendly Version

Interactive Discussion



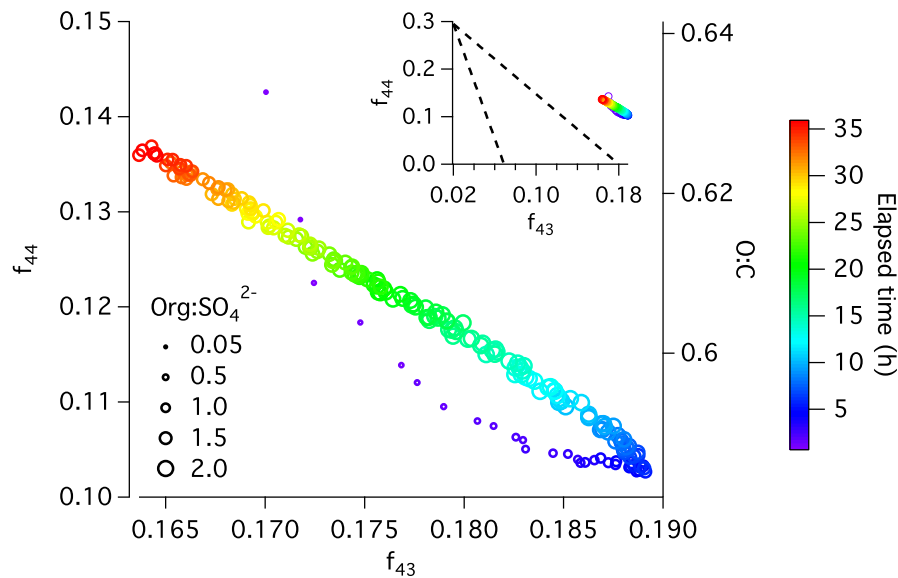


Fig. 3. Evolution of f_{43} , f_{44} , and O:C for 36 h of OH exposure. This system lies to the right of the triangular region in which typical ambient aerosol resides, as shown by the dashed lines in the inset (Ng et al., 2010).

[Title Page](#)
[Abstract](#)
[Introduction](#)
[Conclusions](#)
[References](#)
[Tables](#)
[Figures](#)
[◀](#)
[▶](#)
[◀](#)
[▶](#)
[Back](#)
[Close](#)
[Full Screen / Esc](#)
[Printer-friendly Version](#)
[Interactive Discussion](#)


***m*-Xylene SOA aging**

C. L. Loza et al.

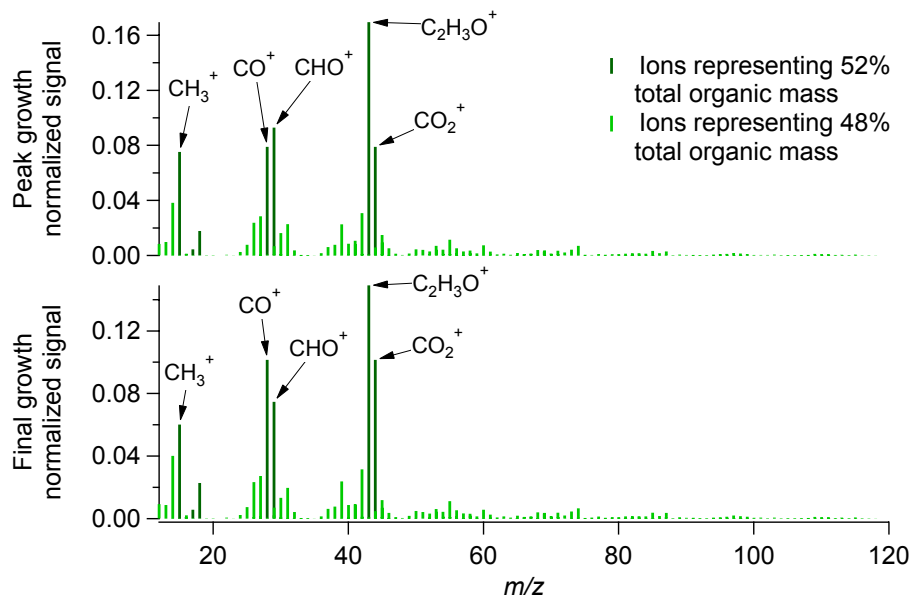


Fig. 4. Average AMS high-resolution organic mass spectra at the time of peak growth and at the end of the experiment (final growth) for the 36-h aging experiment. Prominent peaks are identified. The mass of CO^+ is estimated to equal that of CO_2^+ .

[Title Page](#)[Abstract](#)[Introduction](#)[Conclusions](#)[References](#)[Tables](#)[Figures](#)[◀](#)[▶](#)[◀](#)[▶](#)[Back](#)[Close](#)[Full Screen / Esc](#)[Printer-friendly Version](#)[Interactive Discussion](#)

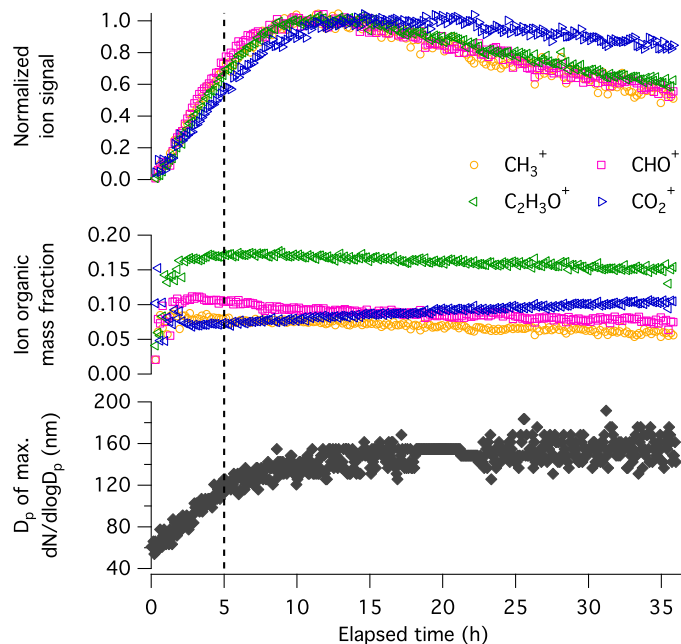


Fig. 5. Evolution of SOA chemical composition from high-resolution AMS measurements and diameter of the maximum number distribution of suspended particles. In the top panel, the ion signal is normalized by sulfate to account for particle wall losses. The sulfate-normalized ion signal is then scaled by the average value at the peak concentration. The middle panel shows the fractional contribution of each ion to the total organic mass signal. A relative ionization efficiency of 1.4 is used when calculating the organic ion concentration. The dashed line at 5 h corresponds to the reversal in trend of O:C.

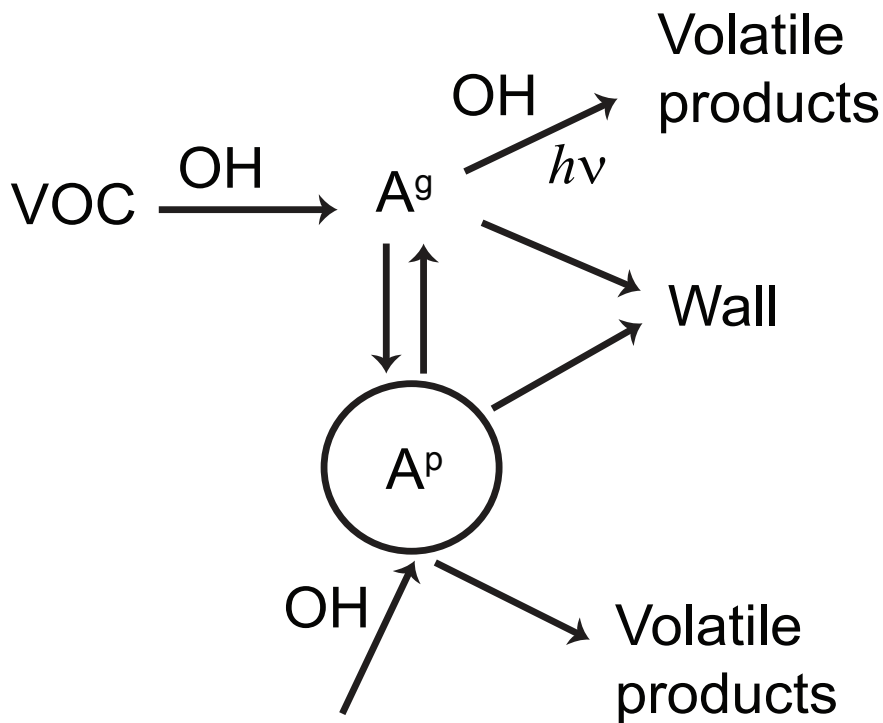


Fig. 6. Sources and sinks of a semivolatile gas-phase species, A^g , and particles containing the condensed semivolatile species, A^p , during SOA aging. We do not explicitly indicate in the sketch processes by which the particle-phase A^p attains a semisolid state, greatly affecting continued exchange with the gas phase (Virtanen et al., 2010; Vaden et al., 2010, 2011; Shiraiwa et al., 2011).

Title Page

Abstract

Introduction

Conclusions

References

Tables

Figures

◀

▶

◀

▶

Back

Close

Full Screen / Esc

Printer-friendly Version

Interactive Discussion



***m*-Xylene SOA aging**

C. L. Loza et al.

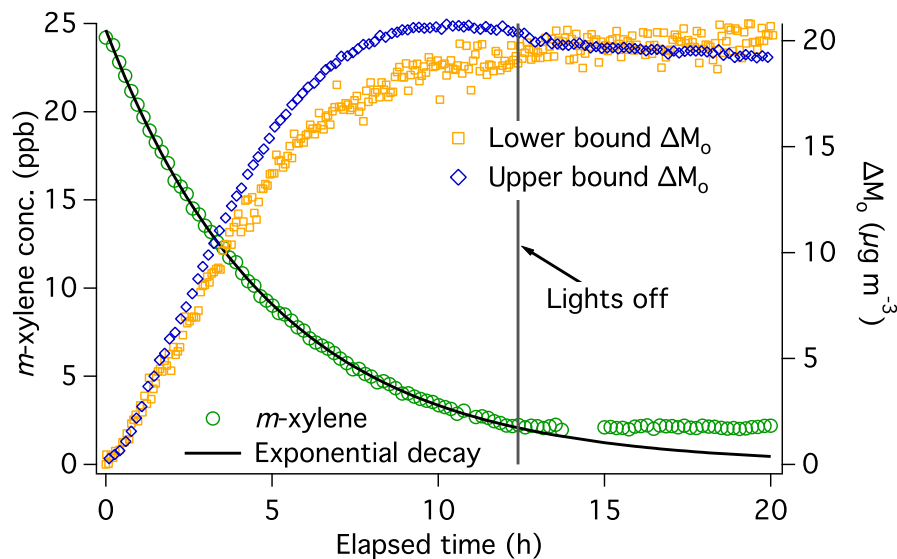


Fig. 7. Trends in *m*-xylene concentration (left axis) and ΔM_0 (right axis) when irradiation is stopped once peak ΔM_0 is attained.

[Title Page](#)[Abstract](#)[Introduction](#)[Conclusions](#)[References](#)[Tables](#)[Figures](#)[◀](#)[▶](#)[◀](#)[▶](#)[Back](#)[Close](#)[Full Screen / Esc](#)[Printer-friendly Version](#)[Interactive Discussion](#)

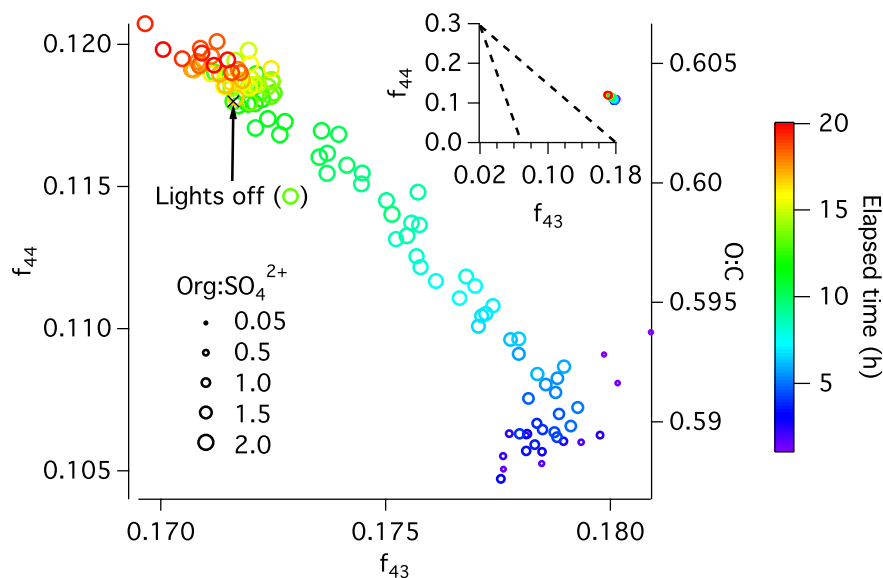
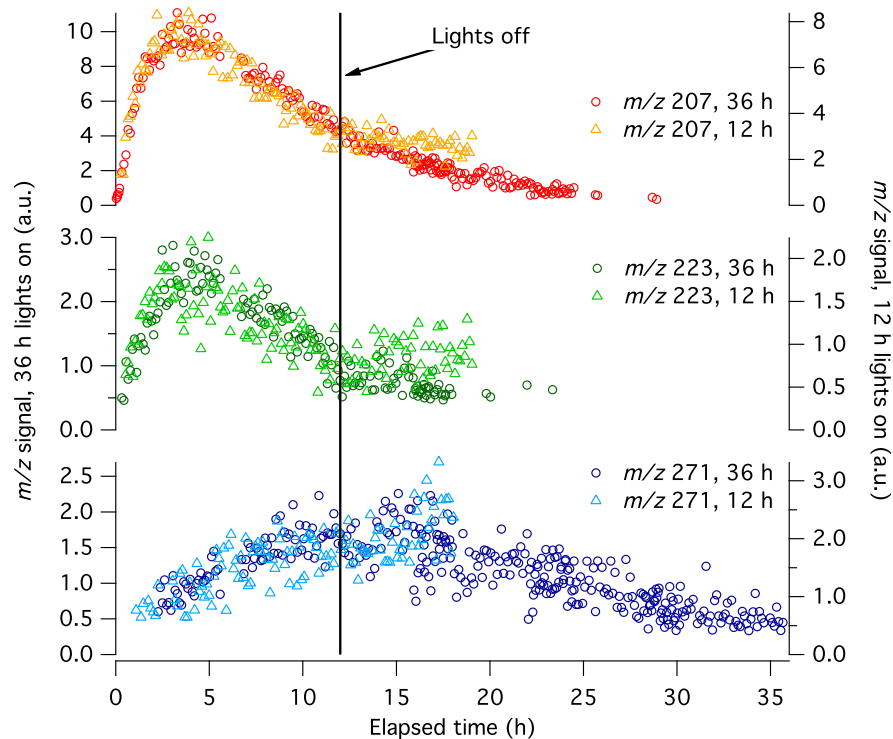


Fig. 8. Evolution of f_{43} , f_{44} , and O:C of *m*-xylene SOA. Irradiation was stopped after 12.4 h, corresponding to the peak of ΔM_o . This point is denoted by the “x”. After irradiation stops, the chemical composition of the SOA does not change significantly. The inset shows the position of the data with respect to the triangular region characteristic of ambient SOA bounded by the dashed lines, as defined by Ng et al. (2010).

[Title Page](#)
[Abstract](#)
[Introduction](#)
[Conclusions](#)
[References](#)
[Tables](#)
[Figures](#)
[◀](#)
[▶](#)
[◀](#)
[▶](#)
[Back](#)
[Close](#)
[Full Screen / Esc](#)
[Printer-friendly Version](#)
[Interactive Discussion](#)


***m*-Xylene SOA aging**

C. L. Loza et al.

**Fig. 9.** Time evolution of products formed during *m*-xylene oxidation detected by the CIMS.

Title Page

Abstract

Introduction

Conclusions

References

Tables

Figures

◀

▶

◀

▶

Back

Close

Full Screen / Esc

Printer-friendly Version

Interactive Discussion



***m*-Xylene SOA aging**

C. L. Loza et al.

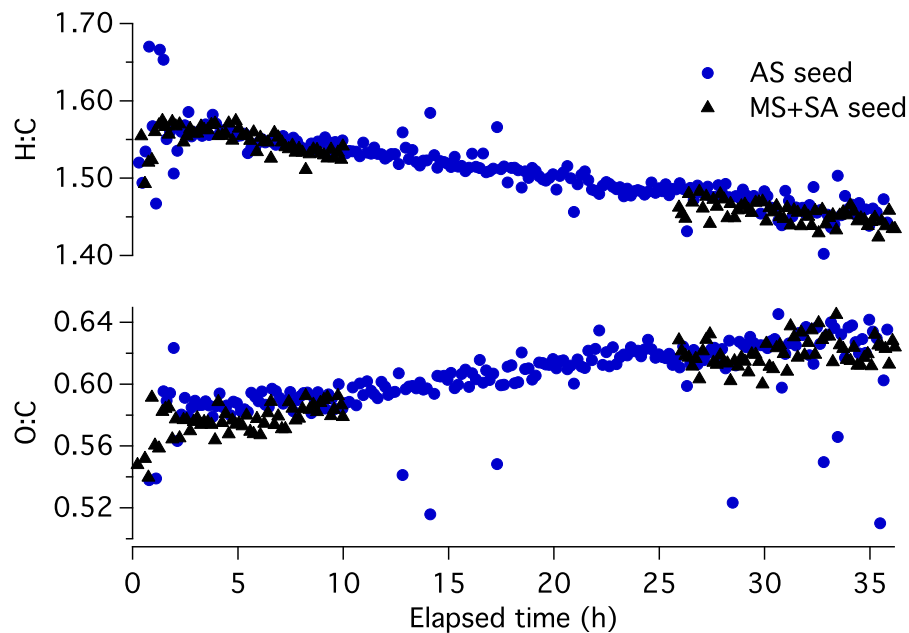


Fig. 10. Elemental ratios of *m*-xylene aerosol condensed onto neutral (AS) and acidic (MS+SA) seed particles.

[Title Page](#)[Abstract](#)[Introduction](#)[Conclusions](#)[References](#)[Tables](#)[Figures](#)[◀](#)[▶](#)[◀](#)[▶](#)[Back](#)[Close](#)[Full Screen / Esc](#)[Printer-friendly Version](#)[Interactive Discussion](#)